Disordered-to-ordered transitions in assembly factors allow the Complex II catalytic subunit to switch binding partners

Pankaj Sharma,[1] Elena Maklashina,[2,3] Markus Voehler,[4,5] Sona Balintova[6], Sarka Dvorakova[6], Michal Kraus[6], Katerina Hadrava Vanova[6,7], Zuzana Nahacka[6], Renata Zobalova,[6] Stepana Boukalova,[6] Tomas Mracek,[8] Hans K. Ghayee,[9] Karel Pacak,[7] Jakub Rohlena,[6] Jiri Neuzil[6,10,11,12,*], Gary Cecchini[2,3,*], T. M. Iverson[1,5, 13,14,*]

Departments of [1]Pharmacology, [4]Chemistry, and [13]Biochemistry, [5]Center for Structural Biology, and [14]Vanderbilt Institute of Chemical Biology, Vanderbilt University, Nashville, TN 37232, USA

[2]Molecular Biology Division, San Francisco VA Health Care System, San Francisco, CA 94121, USA

[3]Department of Biochemistry & Biophysics, University of California, San Francisco, CA 94158, USA

[6]Institute of Biotechnology, Czech Academy of Sciences, 252 50 Prague-West, Czech Republic,

[7]*Eunice Kennedy Shriver* National Institute of Child Health and Human Development, National Institutes of Health, Bethesda, MD, 20814, USA

[8]Institute of Physiology, Czech Academy of Sciences, Prague 4, 142 20 Czech Republic

[9]Department of Medicine, Division of Endocrinology & Metabolism, University of Florida College of Medicine and Malcom Randall VA Medical Center, Gainesville, FL, 32608, USA [10]School of Pharmacy and Medical Science, Griffith University, Southport, Qld 4222, Australia

[11]Faculty of Science and [12]1st Faculty of Medicine, Charles University, 128 00 Prague 2, Czech Republic

[14]Lead contact: tina.iverson@vanderbilt.edu (T.M.I.)

[*]Correspondence: tina.iverson@vanderbilt.edu (T.M.I.), Gary.Cecchini@ucsf.edu (G.C.), j.neuzil@griffith.edu.au or jiri.neuzil@ibt.cas.cz

(J.N.)

Supplementary Information

1. Supplementary Tables 1-3
2. Supplementary Figures 1 - 15

Supplementary Tables 1 - 3

Supplementary Table 1. Crystallographic data collection and refinement statistics. Numbers in parentheses indicate values for the highest resolution shell of data.

	SDHA-SDHAF2-SDHAF4	SDHA-SDHAF4
Data collection		
Space group	$P2_12_12_1$	$P2_12_12$
Cell dimensions		
a, b, c (Å)	66.0, 103.2,126.2	139.0, 69.3, 72.6
α, β, γ (°)	90, 90, 90	90, 90, 90
Resolution (Å)	50-1.52 (1.56-1.52)	50-1.45 (1.51-1.45)
R_{sym}	0.081 (0.970)	0.096 (1.421)
R_{pim}	0.041 (0.491)	0.041 (0.614)
I/σ	24.5 (1.7)	35.6 (1.5)
Completeness (%)	91.7 (89.0)	99.8 (100)
Redundancy	4.2 (4.1)	7.0 (6.2)
$CC_{1/2}$	0.904 (0.648)	0.998 (0.544)
Refinement		
Resolution (Å)	35.5-1.52	28.5-1.45
No. reflections	122165	125470
R_{work}/R_{free}	0.157/0.184	0.154/0.171
No. atoms		
Protein	6083	5185
Water	518	423
B-factors (mean)		
Protein	23.09	26.44
Water	32.63	36.12
RMS deviations		
bond lengths (Å)	0.008	0.008
bond angles (°)	1.02	0.972

Single crystal was used for each structure. Values in parentheses are for highest-resolution shell.

Supplementary Table 2. Inter-protein interactions in the SDHA-AF2-AF4 assembly intermediate.

S. No.	SDHA	Length	SDHAF2
1	K92 (O)	2.73	Y72(O_{η})
2	T96(O_{γ}^{1})	2.82	S113(O)
3	R97(N_{η}^{1})	2.89	P112(O)
4	R97(N_{η}^{2})	2.87	P112(O)
5	H99(N_{δ}^{1})	3.36	G78(O)
6	V101(O)	2.93	W116(N_{ε}^{1})
7	Q104(N_{ε}^{2})	3.21	Y120(O_{η})
8	R195(N_{η}^{1})	3.19	D46(O_{δ}^{2})
9	R195(N_{η}^{2})	2.41	D46(O_{δ}^{1})
10	H198(N_{ε}^{2})	2.77	S113(O_{γ})
11	S199(O_{γ})	2.77	D46(O_{δ}^{2})
12	H202(N_{δ}^{1})	3.13	S113(O_{γ})
13	H202(N_{ε}^{2})	2.73	I50(O)
14	R210(N_{η}^{2})	3.31	P51(O)
15	E240(O_{ε}^{2})	2.88	R58(N_{η}^{1})
16	E240(O_{ε}^{2})	2.64	R58(N_{η}^{2})
17	H270(O)	2.97	K76(NZ)
18	M388(O)	2.93	N146(N_{δ}^{2})
19	F390(O)	2.78	R152(N)
20	E398(O_{ε}^{1})	3.11	K149(N_{ζ})
21	R507(N_{η}^{1})	2.86	E163(O_{ε}^{1})
22	S509(O_{γ})	2.68	E159(O_{ε}^{2})
23	R512(N_{η}^{2})	3.04	D157(O_{δ}^{1})
24	E564(O_{ε}^{1})	2.92	R75(N_{η}^{2})
25	E564(O_{ε}^{2})	2.79	R75(N_{ε})
26	E564(O_{ε}^{2})	2.79	K76(N_{ζ})
27	E567(O_{ε}^{1})	2.70	K76(N_{ζ})
			SDHAF4
1	Q104(O_{ε}^{1})	2.98	R104(N_{η}^{1})
2	Q104(O_{ε}^{1})	3.30	R104(N_{η}^{2})
3	S161(O_{γ})	2.73	E84(O_{ε}^{2})
4	R162(N)	2.92	K85(O)
5	R162(O)	2.83	K85(N)
6	R171(N_{ε})	2.76	E92(O_{ε}^{2})
7	R171(N_{η}^{1})	2.82	E84(O_{ε}^{2})
8	R171(N_{η}^{2})	2.92	E84(O_{ε}^{1})
9	R171(N_{η}^{2})	2.87	E92(O_{ε}^{1})
10	A193(N)	3.13	G86(O)
11	D194(O_{δ}^{1})	2.79	R101(N_{η}^{1})
12	D194(O_{δ}^{2})	3.03	R89(N)
13	L306(O)	2.79	C105(N)
14	T308(N)	2.88	G103(O)
15	T308(O_{γ}^{1})	2.65	D98(O_{δ}^{2})
16	R379(O)	2.84	R95(N_{η}^{2})
17	A454(N)	2.99	D107(O_{δ}^{2})
18	L306(O)	2.79	C105(N)
19	T308(N)	2.88	G103(O)
20	T308(O_{γ}^{1})	2.65	D98(O_{δ}^{2})
21	R379(O)	2.84	R95(N_{η}^{2})
22	T386(O_{γ}^{1})	2.93	K102(O)

Supplementary Table 3. Inter-protein interactions in the SDHA-AF4 assembly intermediate.

S. No.	SDHA	Length	SDHAF4
1	Q104(O_{ε}^{1})	2.82	R104(N_{η}^{2})
2	S161(O_{γ})	2.61	E84(O_{ε}^{2})
3	R162(N)	2.95	K85(O)
4	R162(O)	2.84	K85(N)
5	R171(N_{ε})	2.82	E92(O_{ε}^{2})
6	R171(N_{η}^{1})	2.86	E84($O_{\varepsilon}2$)
7	R171(N_{η}^{2})	2.89	E84(O_{ε}^{1})
8	R171(N_{η}^{2})	2.89	E92(O_{ε}^{1})
9	A193(N)	3.10	G86(O)
10	D194(O_{δ}^{1})	2.81	R101(N_{η}^{1})
11	D194(O_{δ}^{2})	2.93	R89(N)
12	H407(N_{ε}^{2})	3.28	D107(O_{δ}^{1})
13	R451(N_{η}^{1})	2.78	D107(O_{δ}^{1})
14	R451(N_{η}^{2})	3.08	D107(O_{δ}^{1})
15	R451(N_{η}^{2})	3.04	F108(OXT)
16	A454(N)	2.96	D107(O_{δ}^{2})
17	L306(O)	2.83	C105(N)
18	T308(N)	2.88	G103(O)
19	T308(O_{γ}^{1})	2.82	D98(O_{δ}^{1})
20	E309(N)	2.91	D98(O_{δ}^{2})
21	E314(O_{ε}^{2})	2.60	Y96(O_{η})
22	R379(O)	3.12	R95(N_{η}^{2})
23	E385(O_{ε}^{1})	2.85	E69(N)
24	E385(O_{ε}^{1})	2.99	K102(N_{ζ})
25	T386(O_{γ}^{1})	2.68	K102(O)

Supplementary Figures 1 – 15

Supplementary Figure 1

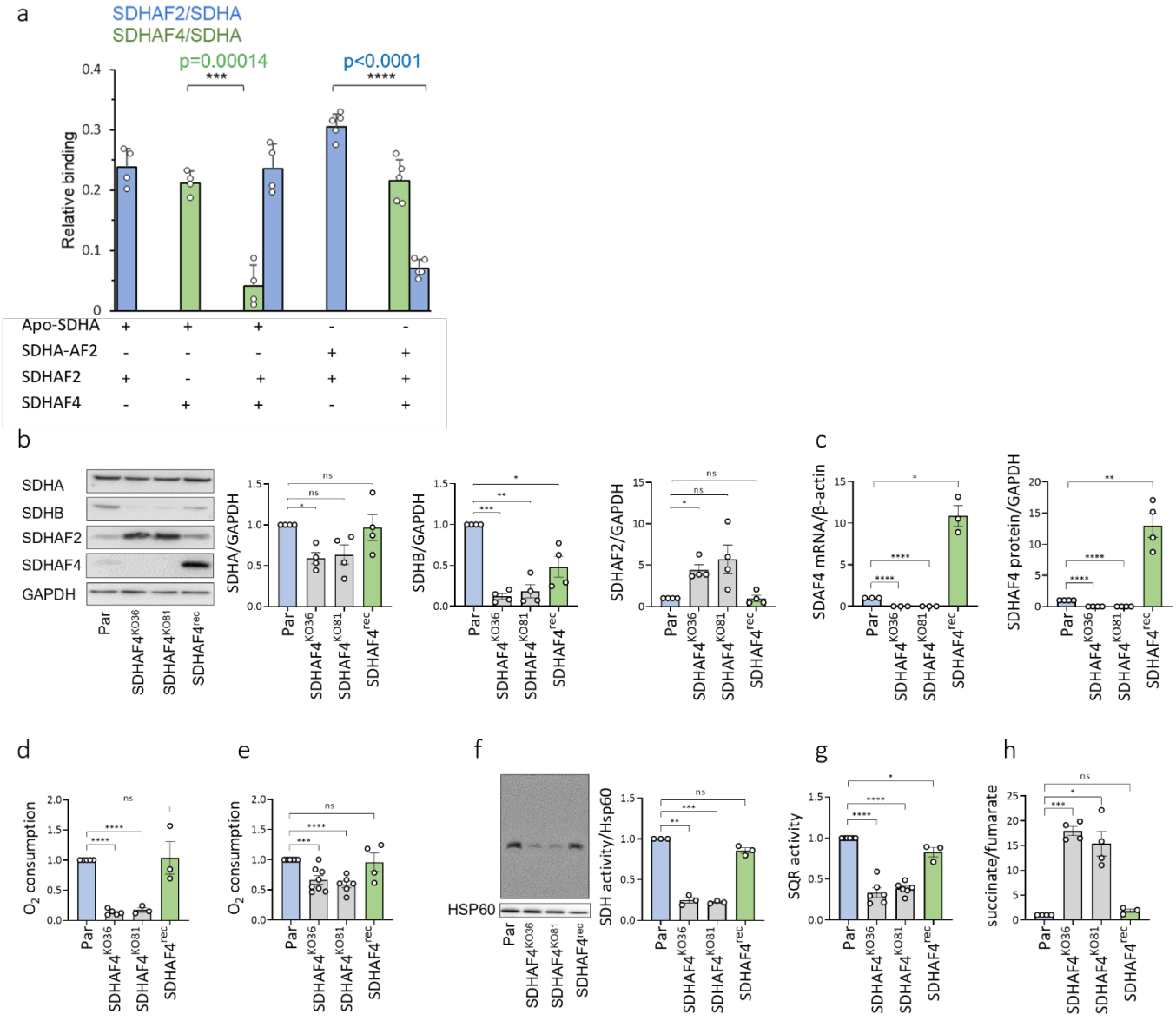

Figure S1. Validation of cell lines with perturbed SDHAF4. (a) Quantitation of the gel shown in Figure 2a by densitometry and ImageJ [3]. **(b)** Measurement of levels of relevant CII subunits and assembly factors in duplicate SDHAF4^{KO} cell lines. (left) Parental, SDHAF4^{KO36}, SDHAF4^{KO81} and SDHAF4^{rec} cells were subjected to SDS-PAGE followed by western blotting using anti-SDHA, anti-SDHB, anti-SDHAF2 and anti-SDHAF4 IgG. GAPDH levels measured using anti-GAPDH IgG, was used as loading control. (right) Quantitation of individual proteins assessed by western blotting related to GAPDH. **(c)** Parental, SDHAF4^{KO36}, SDHAF4^{KO81} and SDHAF4^{rec} cells were evaluated by (left) qRT-PCR for the level of SDHAF4 mRNA, related to β-actin mRNA, or (right) by densitometry of the westerns in panel **(b)**. **d) - f)** Parental, SDHAF4^{KO36}, SDHAF4^{KO81} and SDHAF4^{rec} cells were assessed for **(d)**, routine respiration, **(e)** CII-dependent respiration, **(f)** SDH activity, **(g)** SQR activity, and **(h)** succinate/fumarate ratio. For panel **(f),** the SDH activity was evaluated using high-

resolution clear chromatography followed by in gel activity. The gel image is on the left and densitometric evaluation corrected to HSP60 is on the right. Panel **(f)** shows a representative image of 3 independent experiments. Bar graphs show mean values ± EM (n=3); *, $p<0.05$; **, $p<0.01$; ***, $p<001$; and ****, $p<0.0001$; n.s., non-significant.

The exact *p*-values are: (**b**) SDHA/GAPDH, par. vs. $SDHAF4^{KO36}$ $p=0.0106$, par vs. $SDHAF4^{KO81}$ $p=0.0560$, par. vs. $SDHAF4^{rec}$ $p=0.8496$.; SDHB/GAPDH, par. vs. $SDHAF4^{KO36}$ $p<0.0001$, par vs. $SDHAF4^{KO81}$ $p=0.0021$, par. vs. $SDHAF4^{rec}$ $p=0.0276$; SDHAF2/GAPDH, par. vs. $SDHAF4^{KO36}$ $p=0.0122$, par vs. $SDHAF4^{KO81}$ $p=0.0726$, par. vs. $SDHAF4^{rec}$ $p=0.9697$ (**c**) SDHAF4 mRNA/β-actin, par. vs. $SDHAF4^{KO36}$ $p<0.0001$, par vs. $SDHAF4^{KO81}$ *p*.0001, par. vs. $SDHAF4^{rec}$ $p=0.0155$; SDHAF4 protein/GAPDH, par. vs. $SDHAF4^{KO36}$ $p<0.0001$, par vs. $SDHAF4^{KO81}$ $p=<0.0001$, par. vs. $SDHAF4^{rec}$ $p=0.008$ **(d)** parental vs. $SDHAF4^{KO36}$ $p<0.0001$, parental vs. $SDHAF4^{KO81}$ $p<0.0001$, parental vs. $SDHAF4^{rec}$ n.s. **(e)** parental vs. $SDHAF4^{KO36}$ $p<0.0001$, parental vs. $SDHAF4^{KO81}$ $p=0.0003$, parental vs. $SDHAF4^{rec}$ $p=0.7915$; **(f)** parental vs. $SDHAF4^{KO36}$ $p=0.0022$, parental vs. $SDHAF4^{KO81}$ $p=0.0002$, parental vs. $SDHAF4^{rec}$ $p=0.0504$; **(g)** parental vs. $SDHAF4^{KO36}$ $p<0.0001$, parental vs. $SDHAF4^{KO81}$ $p<0.0001$, parental vs. $SDHAF4^{rec}$ $p=0.0504$; **(h)** parental vs. $SDHAF4^{KO36}$ $p=0.0003$, parental vs. $SDHAF4^{KO81}$ $p=0.01$, parental vs. $SDHAF4^{rec}$ $p=0.1523$

Supplementary Figure 2.

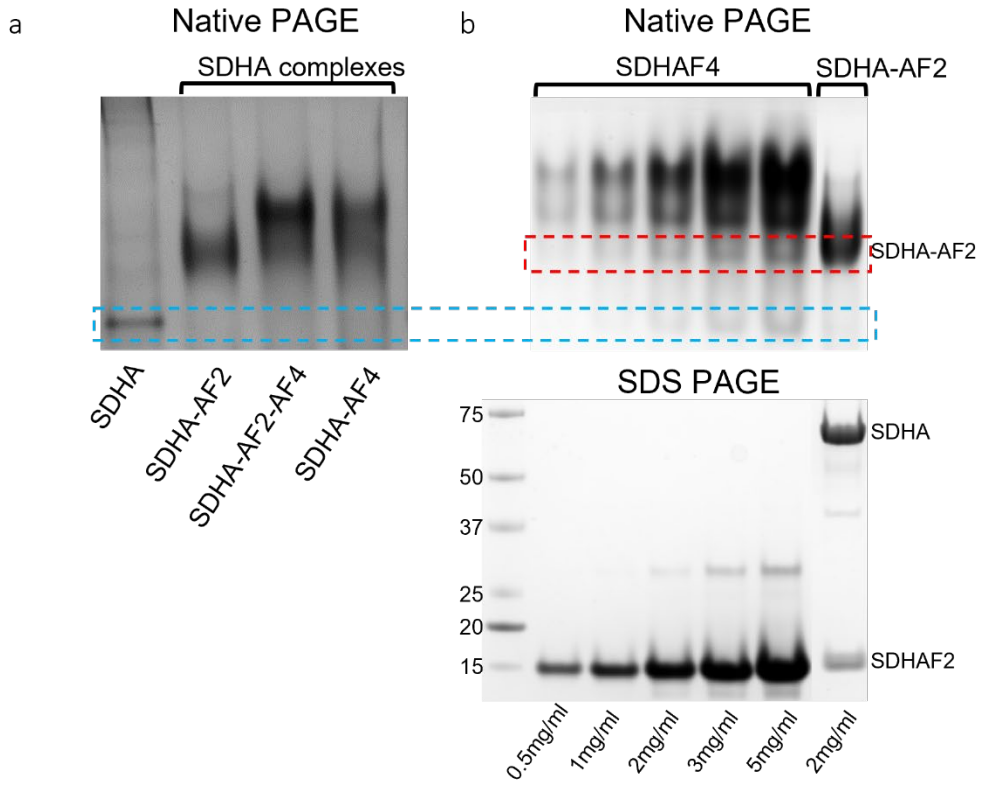

Figure S2. SDHAF4 oligomerization. (a) Migration of purified SDHA, SDHA-AF2, SDHA-AF2-AF4 and SDHA-AF4 on native PAGE. SDHAF4-containing complexes migrate slower than the SDHA-AF2 complex. **(b)** SDHAF4 oligomerization on both native and SDS gels at concentrations between 0.5 – 5 mg/ml. The migration of SDHA-AF2 (2mg/ml) is shown for comparison. Comparison of the native gels in (**a**) and **(b)** identifies that purified SDHAF4 forms oligomers that can migrate at a molecular weight similar to SDHA-AF2 complex (red box) and isolated SDHA (blue box). The SDS-PAGE gel shows that SDHAF4 forms dimers at higher protein concentrations even in denaturing conditions.

Supplementary Figure 3

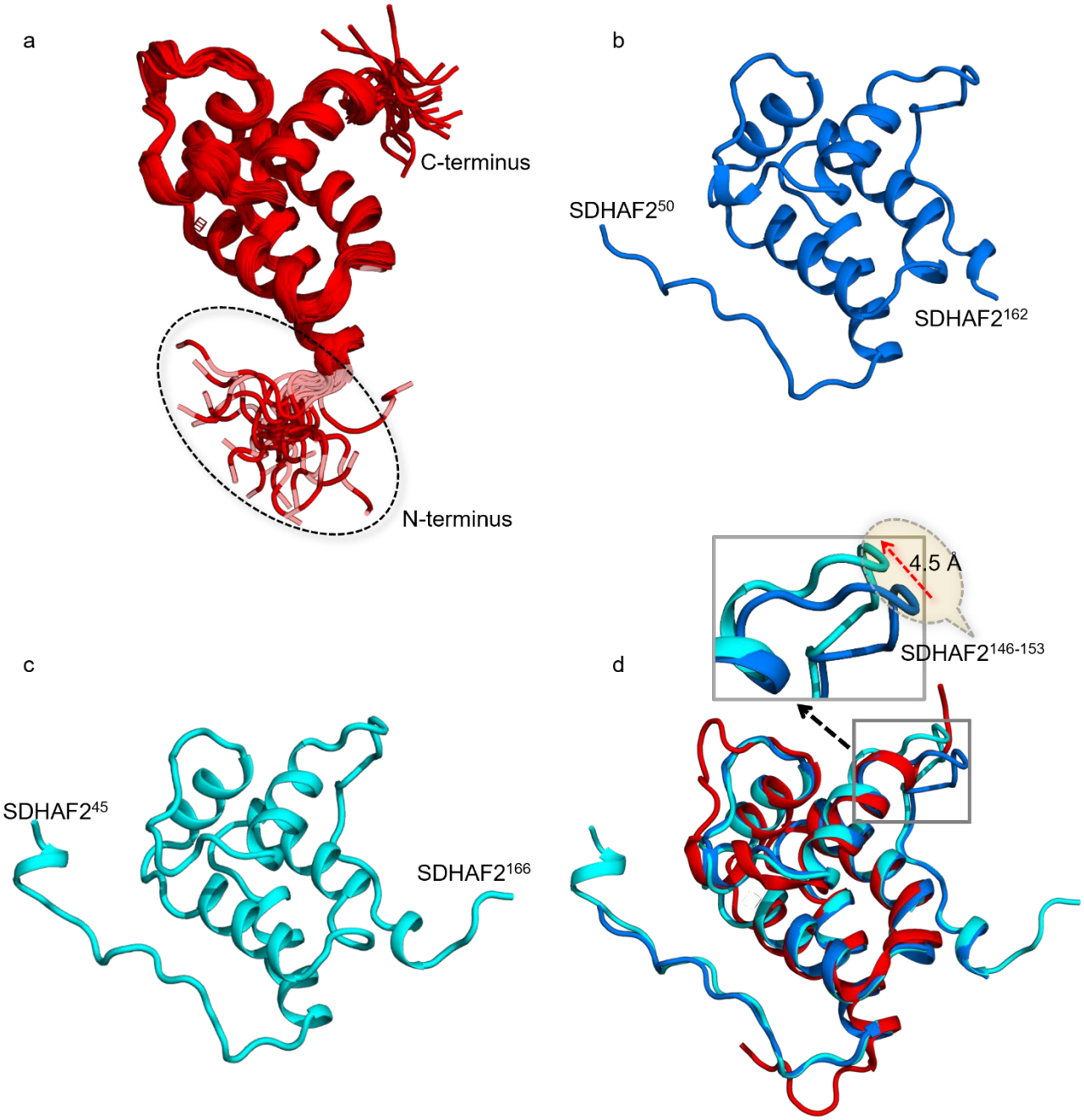

Figure S3. Changes in disorder in SDHAF2 upon binding to SDHA. (a) NMR structure of the yeast SDHAF2 homolog (PDBID 2LM4)[4]; all 20 deposited structures are shown. Both the N- and C-termini exhibit intrinsic disorder. **(b)** Human SDHAF2 resected from the SDHA-AF2 structure (PDB ID 6VAX)[1]. The termini of SDHAF2 when bound to SDHA increase in ordering but lack secondary structure. Full-length SDHAF2 contains residues 1 – 166, and residues are still disordered at both termini. **(c)** SDHAF2 resected from the SDHA-AF2-AF4 structure, reported here. Additional residues at each of the termini gain order compared to SDHA-AF2 structure. Th entire C-terminus is now ordered. **(d)** Comparison of the structures of the isolated yeast SDHAF2 homolog (*red*, single state from 20 deposited structures), human SDHAF2 resected from the SDHA-AF2 structure (*blue*) and human SDHAF2 resected from the SDHA-AF2-AF4 structure (*cyan*).

Differences are observed in the changes in order at the termini and in residues SDHAF2$^{146\text{-}153}$ (*inset*). Note that the termini of the isolated yeast SDHAF2 homolog are disordered, while those of the bound SDHAF2 are ordered, but lack secondary structure.

Supplementary Figure 4

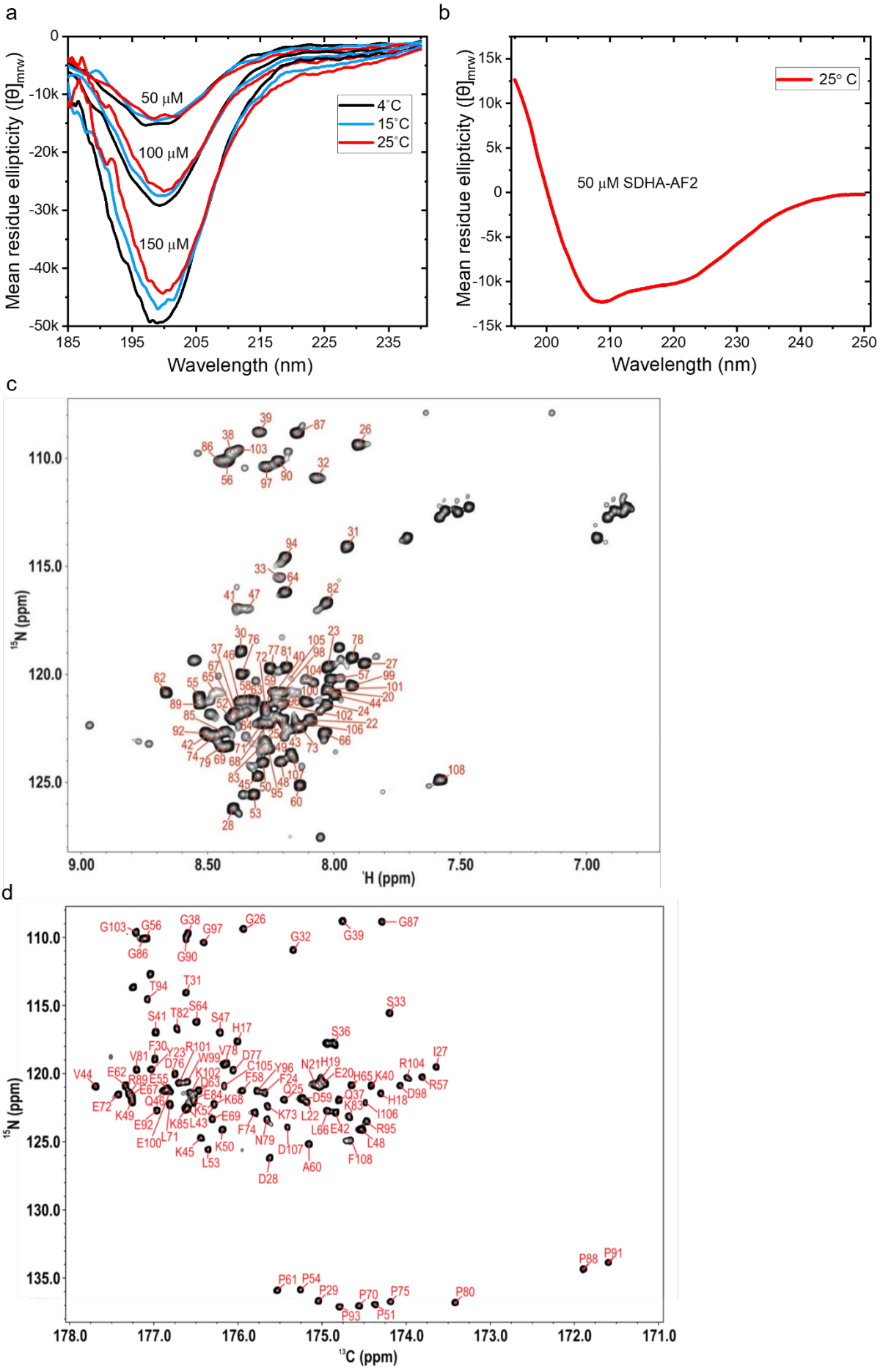

Figure S4. Isolated SDHAF4 is an intrinsically disordered protein. (a) Circular dichroism spectra of SDHAF4 collected at three temperatures (4 °C, 15 °C and 25 °C) and three protein concentrations (50 μM, 100 μM and 150 μM) all show a peak minimum at 200 nm, suggesting that SHDAF4 is an intrinsically disordered protein. **(b)** As a comparator for the CD spectrum of SDHAF4, we collected a circular dichroism spectrum of the SDHA-AF2 complex (50 μM) collected at 25 °C. The spectrum shows clear differences from the disordered SDHAF4 and is consistent with a folded protein, with minima at 208 and 222 nm and at 218 nm reflecting the presence of α-helices and β-strands, respectively. **(c)** Full 15N-1H HSQC spectrum with assigned peaks transferred from the assignments of the carbon direct detect spectra via the HNCO. The N-terminal His-tag and sidechain as well as peaks from a putative minor conformation were not assigned. **(d)** The carbon direct detects CON spectrum with full assignment of all residues.

Supplementary Figure 5

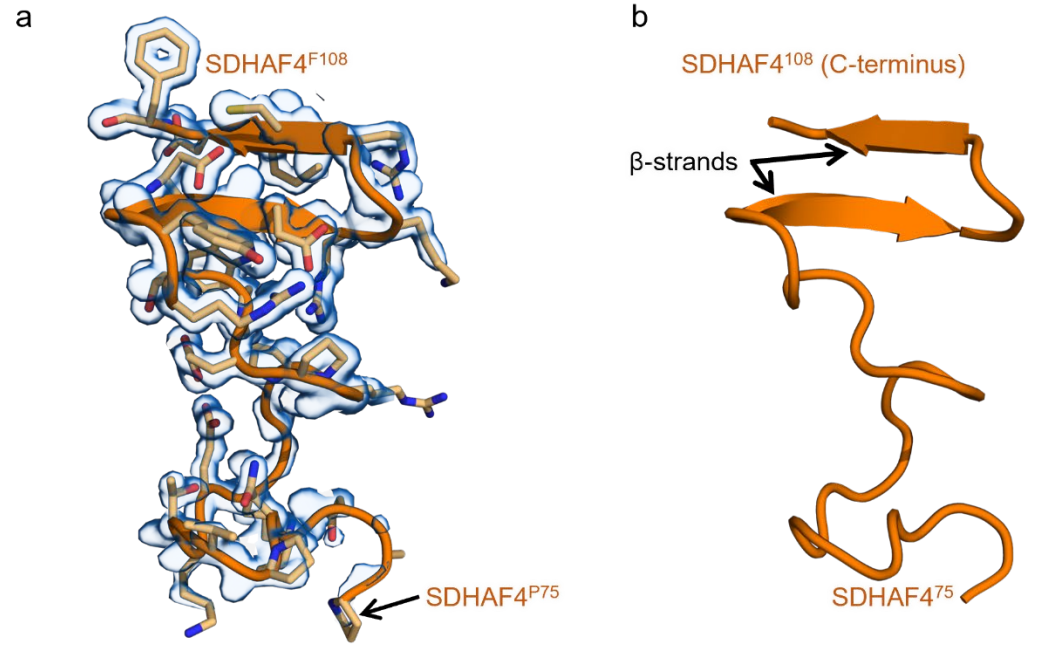

c

```
HUMAN                ------MTPSRLPWL----------LSWVSATAWRAARS--PL-LCHSLRKTS---S-SQ  37
Rhodobacteraceae     ------------------------------------------------------------  0
Saccharomyces        MLCAIKSTGYRYPRTGALNLLRGRPFNMATRKITTERIPGPPKLPREEQEEFERLQRIAT  60
Drosophila           MQSVTRQTARVLPQVGK------QVSYLSTSGAWRASAGGSDM-VVEIKEPK------T-  46
Arabidopsis          --------------------------MATNNIVRLIAPSRSV-SSRFLEPVS---RFLS  29
Danio                ----------------------------------------M-NTAGLRPAG---Y-A-  12
Gallus               --------------------------MALRLLRAAARS--SL-PCSSVRSY------TS  24

HUMAN                GGKSE-----L-----VKQSLKKPKLPEGRFDAP-ED--SHLEKEPLEKFPDDVNPVTKE  84
Rhodobacteraceae     ----------M-----TE--ETRKDLPPEALRALAEA--E------ERRRQAKALDLPKE  35
Saccharomyces        SQEAIDQYNAQATADRTKESLNSPLLTKNDIGSF-----SPEFSKTIPEFEGDVNPKTGE  115
Drosophila           RTEKL-----M-----AFQKKLRAKTPLGKLDEFSRH--PYQEKEPLKPWPNQTNPYTGE  94
Arabidopsis          SGTPP-----PPQAPSPNQDLNRDVKPDQNLQQNLQMQKEEEEEGEGGGGGEFVNEDTGE  84
Danio                SGGVT-----K-----DKEPLKKAKTPQGRFDME-ET--ESKSKDVLERFPDDVNPETKE  59
Gallus               EGRPE-----P-----AKQTLKKPKLPVGRFDEP-KE--SNIEREPLEKFPDGINPATKE  71
                                                                              *

HUMAN                KGGPRGFEPTRYGDWERKGRCIDF       108
Rhodobacteraceae     IGGRNGFEPVRFGDWEKKGIAIDF       59
Saccharomyces        VGGPK-QDPLRHGDYSFNGRVTDF       138
Drosophila           IGGPAGFEPTRYGDWERKGRVSDF       118
Arabidopsis          IGGPRGFEPTRYGDWEQRGRCSDF       108
Danio                KGGPRGFEPTRYGDWERKGRCIDF       83
Gallus               RGGPKGFEPTRFGDWERKGRCIDF       95
                      **    :* *.**:. .*   **
```

Figure S5. Fold and sequence conservation of SDHAF4. (a) Structure of SDHAF4 resected from the SDHA-AF2-AF4 complex shown with side chains and superimposed onto a $2|F_o|-|F_c|$ electron density map (blue, at 1σ) calculated following molecular replacement but before building the SDHAF4 polypeptide. Only residues SDHAF4$^{75\text{-}108}$ were observed in the context of the SDHA-AF2-AF4 complex. **(b)** Ribbon representation of the SDHAF4 structure (residues 75-108) resected from the SDHA-AF2-AF4 structure. **(c)** Sequence alignment of

SDHAF4 homologs. Comparators are from human, *Rhodobacter sphaeroides, Saccharomyces cerevisiae* (yeast), *Drosophila melanogaster* (fruit fly), *Arabidopsis thaliana* (plant), *Danio rerio* (zebrafish), *Gallus gallus* (chicken). Red boxes highlight conserved residues that were selected for mutation.

Supplementary Figure 6

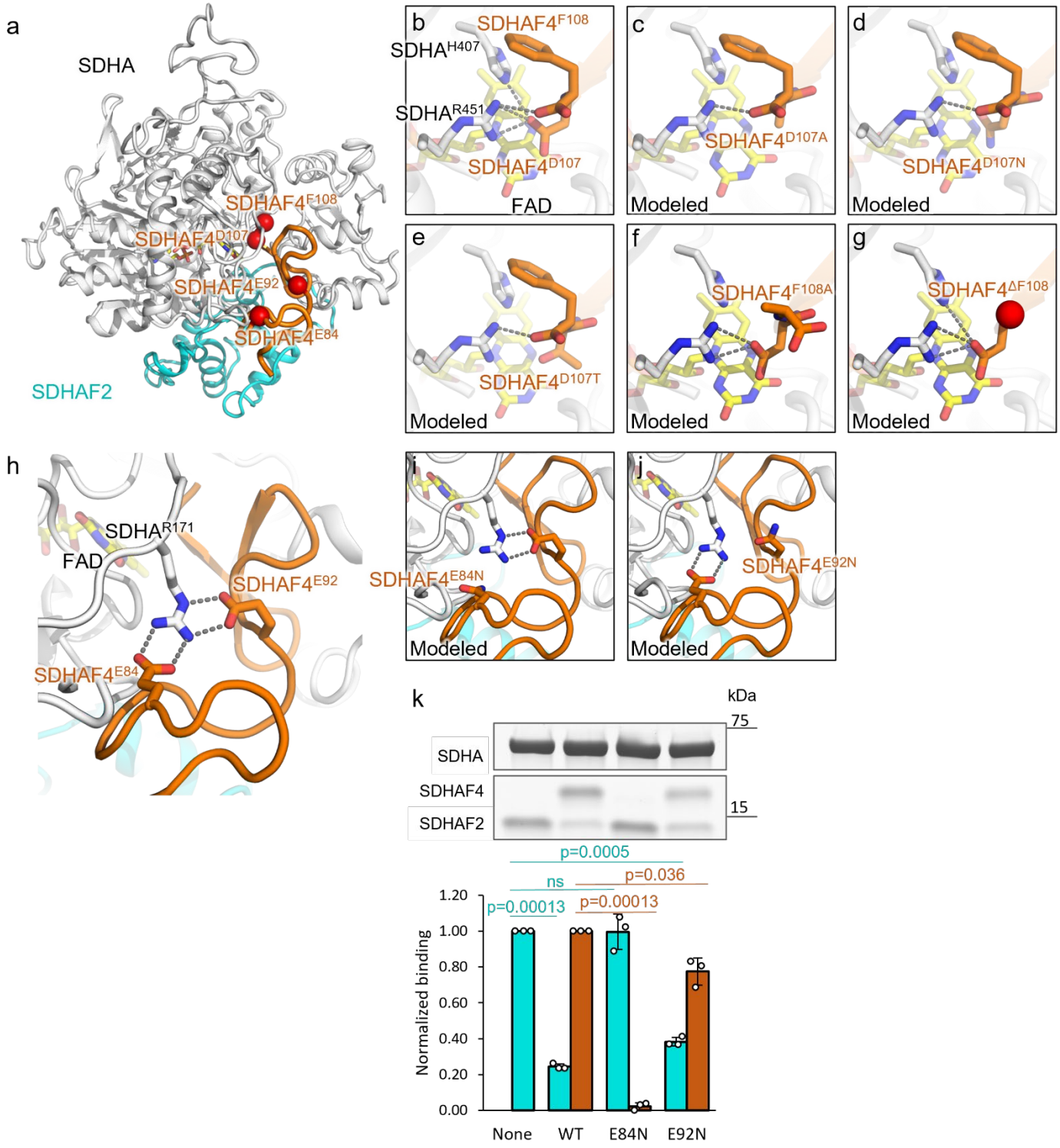

Figure S6. Mutational analysis of SDHAF4. (a) Locations of substitution and truncation mutations of SDHAF4 in the context of the SDHA-AF2-AF4 crystal structure. The affected residues included SDHAF4^{E84}, SDHAF4^{E92}, SDHAF4^{D107}, and SDHAF4^{F108}. **(b)** Interactions between the SDHAF4 C-terminus and the SDHA active site. SDHAF4^{D107} and SDHAF4^{F108} interact with the active site of SDHA including the substrate-interacting residues SDHA^{H407} and SDHA^{R451}. **(c-g)**, Models of the SDHAF4 C-terminal residue mutations. Coot [5] was used to substitute residues. In each case, the most favored rotamer that made reasonable interactions

was hand selected. **(c)** SDHAF4^{D107A}, **(d)** SDHAF4^{D107N}, **(e)** SDHAF4^{D107T}, **(f)** SDHAF4^{F108A} and **(g)** SDHAF4$^{\Delta F108}$. **(h)** detailed interactions between SDHAF4^{E84} and SDHAF4^{E92} with the conserved SDHA^{R171}. **(i-j).** Modeling of **(i),** SDHAF4^{E84N} and **(j)** SDHAF4^{E92N} predicts the disruption of stabilizing interactions between SDHA and SDHAF4. **(k)** Displacement of SDHAF2 from the SDHA-AF2 complex by SDHAF4^{E84N} and SDHAF4^{E92N} showed that SDHAF4^{E84N} did not bind, while SHDHAF4^{E92N} bound but was ~40-50% less efficient.

Supplementary Figure 7

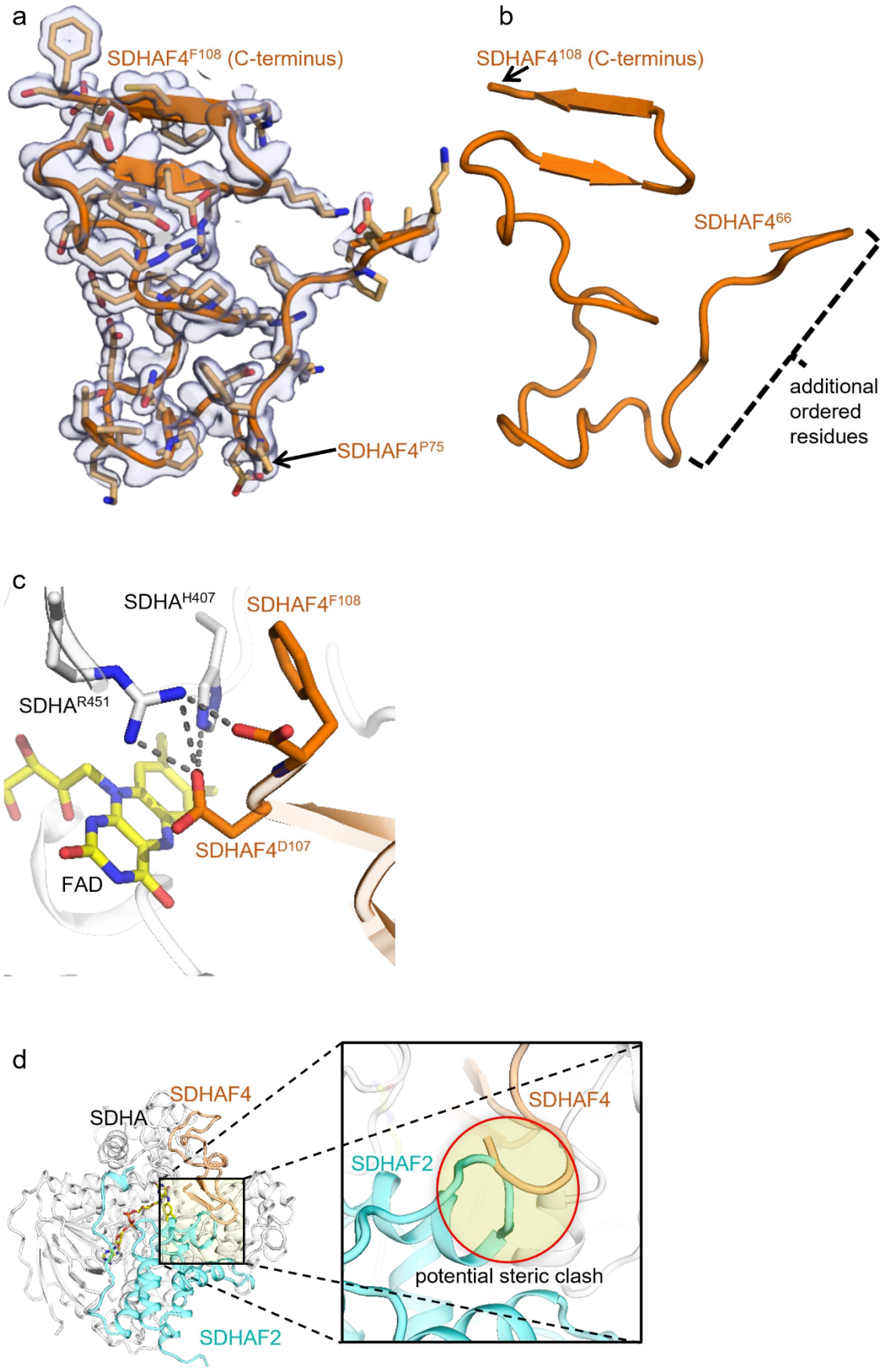

Figure S7. SDHAF4 in the context of the SDHA-AF4 complex. (a) SDHAF4 (*orange*) resected from the SDHA-AF4 complex and superimposed onto a $2|F_o|-|F_c|$ electron density map contoured at 1σ level (*blue*). An additional nine residues of SDHAF4 are ordered in SDHA-AF4 compared to SDHA-AF2-AF4 complex. In the newly ordered region, a tight turn is facilitated by $SDHAF4^{P75}$; mutation of $SDHAF4^{P75}$ is associated with vagal paraganglioma [6]. **(b)** Ribbon representation of the SDHAF4 structure (residues 66-108) resected from the SDHA-AF4 structure. **(c)** Interactions between the active site of SDHA and the C-terminus of SDHAF4 appear to be unchanged when compared to the SDHA-AF2-AF4 structure. **(d)** Superposition of SDHA-AF2-AF4 and SDHA-AF4 highlight region that the additionally ordered regions of SDHAF4 in the SDHA-AF4 structure would be steric conflict with SDHAF2 if it remained bound (*inset*, red circle).

Supplementary Figure 8

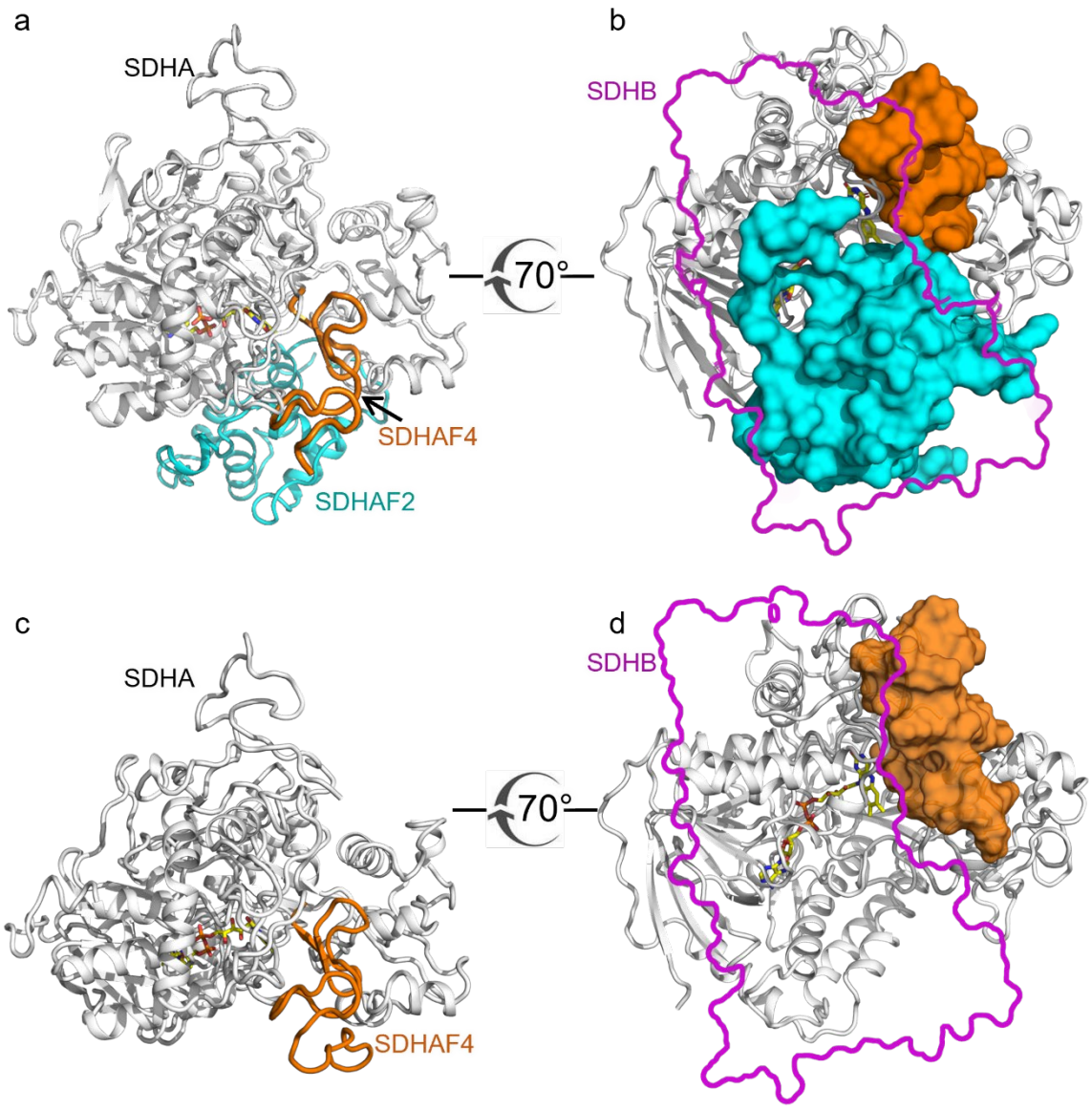

Figure S8. The footprint for SDHB on SDHA overlaps with the binding sites for both the SDHAF2 and the SDHAF4 assembly factor. SDHA is shown in *white*, SDHAF2 is shown in *cyan*, SDHAF4 is shown in *orange*. The footprint where SDHB binds is shown as a pink outline. **(a)** The structure of the SDHA-AF2-AF4 complex shown as ribbons. **(b)** A rotated view of with SDHAF2 and SDHAF4 shown as surfaces and the binding location for SDHB shown as an outline. The location of SDHB was identified by superposition of the porcine CII structure PDB ID 3SFD[7] onto the structure of SDHA-AF2-AF4. **(c)** The structure of the SDHA-AF4 complex shown as ribbons. **(d)** A rotated view of the SDHA-AF4 complex with SDHAF4 shown as surface and the binding location for SDHB shown as an outline. The location of SDHB was identified by superposition of the porcine CII structure PDB ID 3SFD[7] onto the structure of SDHA-AF4.

Supplementary Figure S9

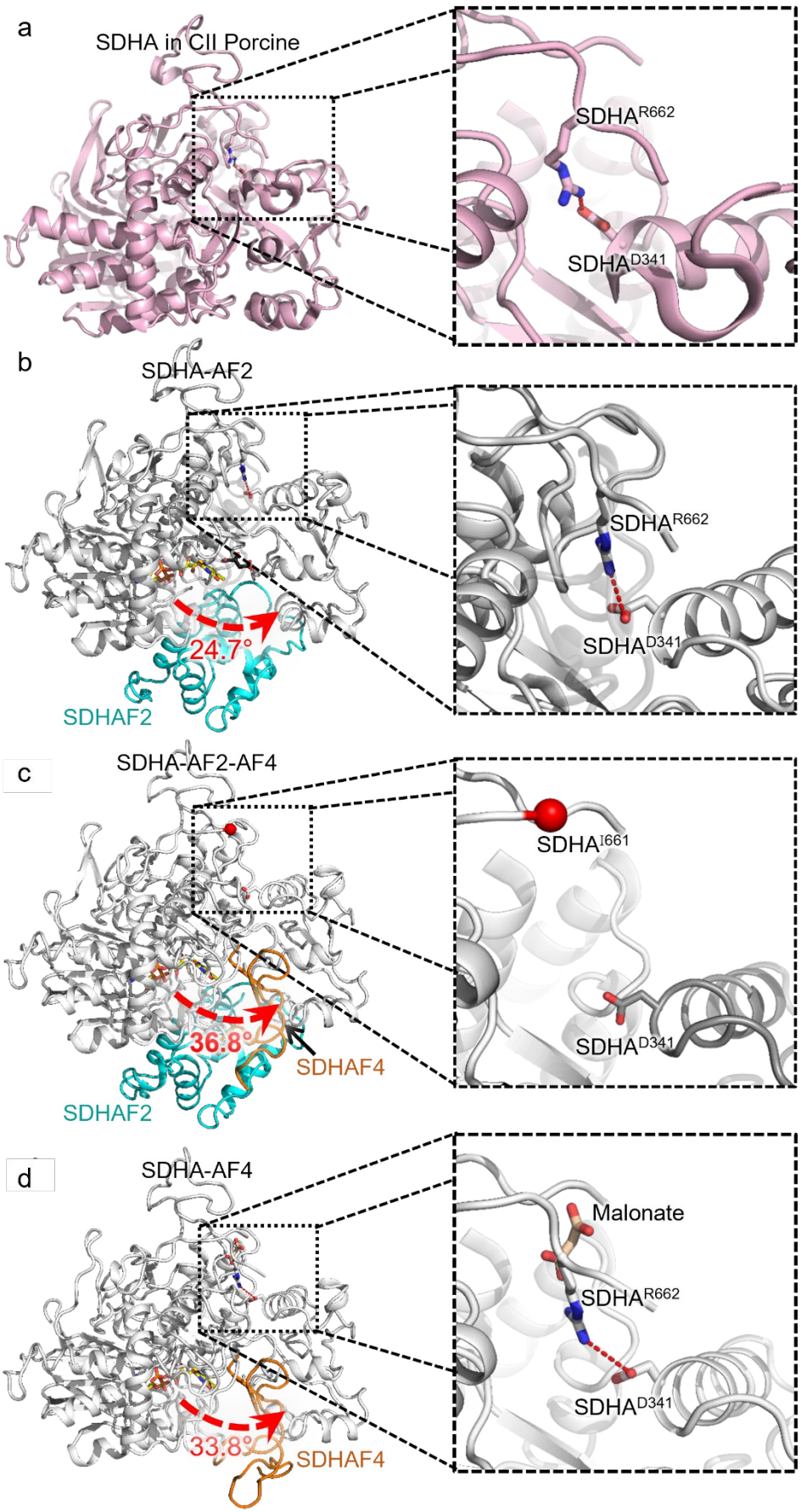

Figure S9. Changes in disorder of SDHA during maturation. Porcine SDHA is shown in *pink*, human SDHA is shown in *white*, human SDHAF2 is shown in *cyan*, and human SDHAF4 is shown in *orange.* The changes in angle of rotation between SDHA flavin binding and capping domains as it binds to assembly factors when compared to SDHA in assembled complex (PDB ID 3SFD[7]) is shown in *red.* **(a)** The structure of SDHA in the context of mature CII (SDHABCD) has been determined from porcine CII, where porcine SDHA is 95% identical and 96% similar to human SDHA. A notable salt bridge between residues $SDHA^{R662}$ and $SDHA^{D341}$ stabilizes the positions of two domains that surround the active site (PDB ID 3SFD[7]). **(b)** The interaction between $SDHA^{R662}$ and $SDHA^{D341}$ is also present in SDHA-AF2 complex (PDB ID 6VAX)[1]. **(c)** However, this salt bridge is disrupted in SDHA-AF2-AF4 complex. As a result, the C-terminal residues of SDHA become disordered after $SDHA^{I661}$ (*red* sphere) and lack associated electron density in the crystal structure. **(d)** This interaction is restored in the SDHA-AF4 complex.

Supplementary Figure 10

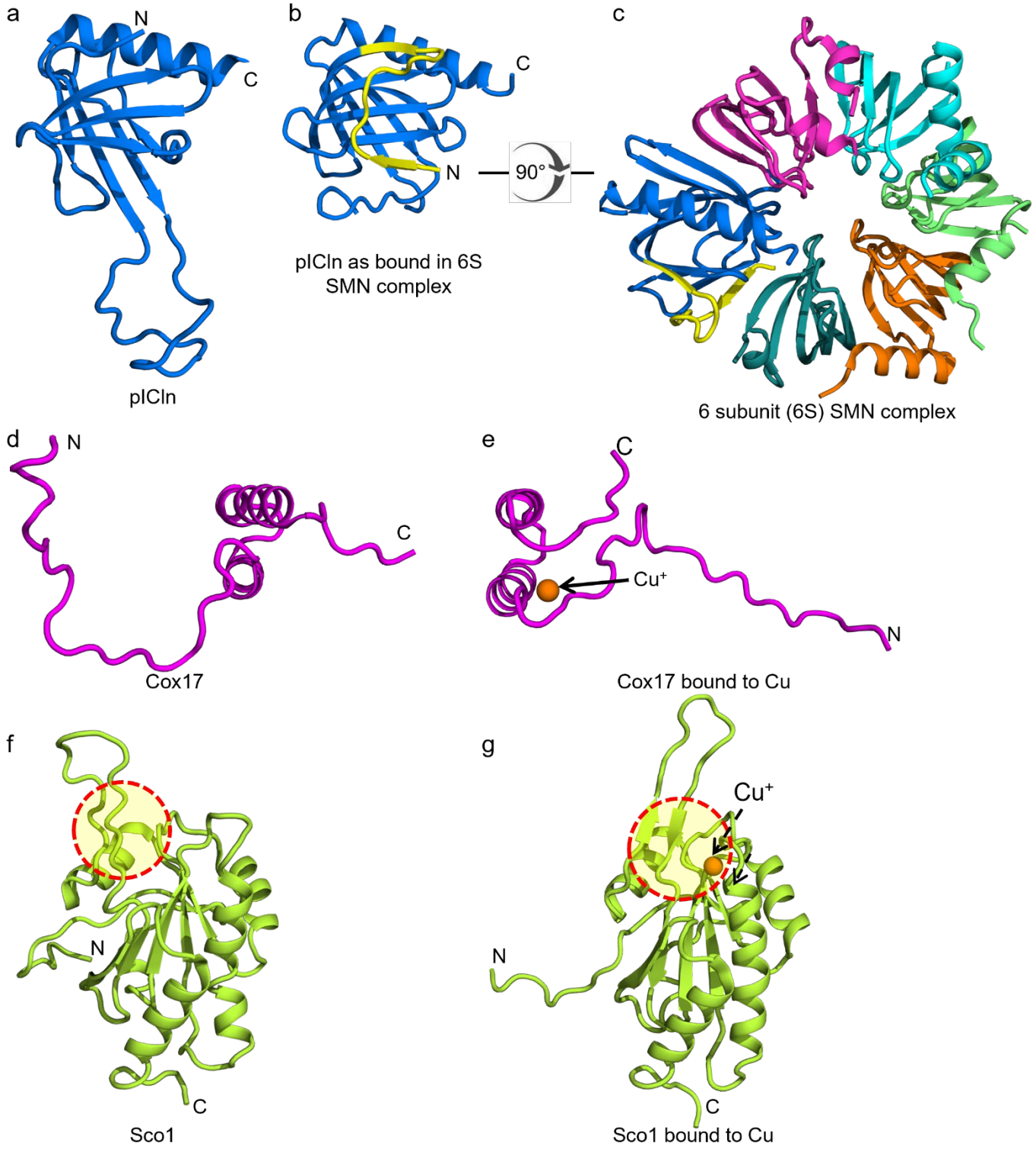

Figure S10 Examples of changes in disorder of assembly factors during biogenesis.

(a) pICln (blue ribbon) is an assembly chaperone for small nuclear ribonucleoproteins. pICln is disordered at its N-terminus as an isolated protein (PDB ID 1ZYI)[8] and contains a long, unstructured loop. **(b)** pICln upon binding to the SMN complex (PDB ID 4F7U)[9] the N-terminus of pICln organizes into a β-strand (yellow ribbon). **(c)** SMN complex with six subunits. The decrease in disorder of the N-terminus of pICln probably stabilizes the assembly intermediate[8,9]. **(d)**

Cox17 is an assembly factor for respiratory complex IV and changes from open conformation (violet ribbon, PDB ID 1U97)[10] to a **(e)** closed conformation (PDB ID 1U96)[10] upon binding to copper[10] (orange sphere). **(f)** Sco1 is involved in the delivery of copper to complex IV. A core loop (red dotted circle) of Sco1 becomes ordered when the isolated polypeptide (lemon ribbon, PDB ID 2GT5)[11] **(g)** binds to the metal ions (Cu as orange sphere, PDB ID 2GQM)[11].

Supplementary Figure 11

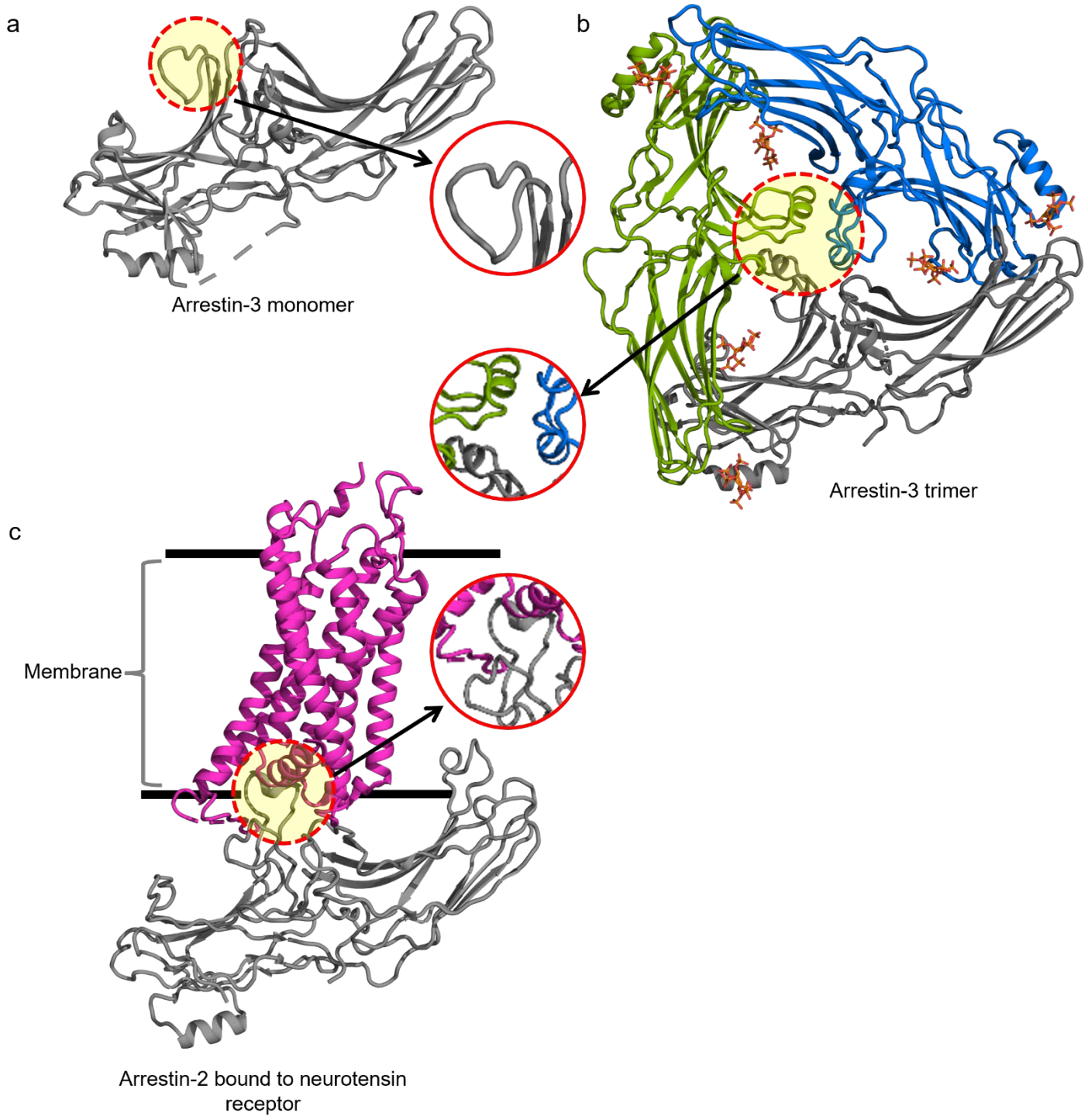

Figure S11. Changes in disorder in the protomers of self-assembling arrestin complexes.

(a) A mammalian signal-transducing protein called arrestin-3 is normally a monomer in solution (grey ribbon, left, PDB entry 3P2D)[12]. An unstructured loop (red dotted circle) is involved in direct interactions to >800 distinct binding partners. **(b)** Interaction with the small molecule inositol hexaphosphate can induce arrestin-3 can trimerization (PDB ID 5TV1)[13]. The unstructured of monomeric arrestin forms an α-helix that mediates trimerization (red dotted circle). **(c)** Structures of the arrestin-2 homolog with the neurotensin receptor (PDB ID 6UP7)[14], which belongs to the family of G protein coupled receptors. The same region of arrestin that forms an

α-helix during self-trimerization now forms a dynamic extended conformation with receptor[14,15]. The plasticity of this region may assist in self-assembly and may promote binding to a broad range of partners.

Supplementary Figure 12

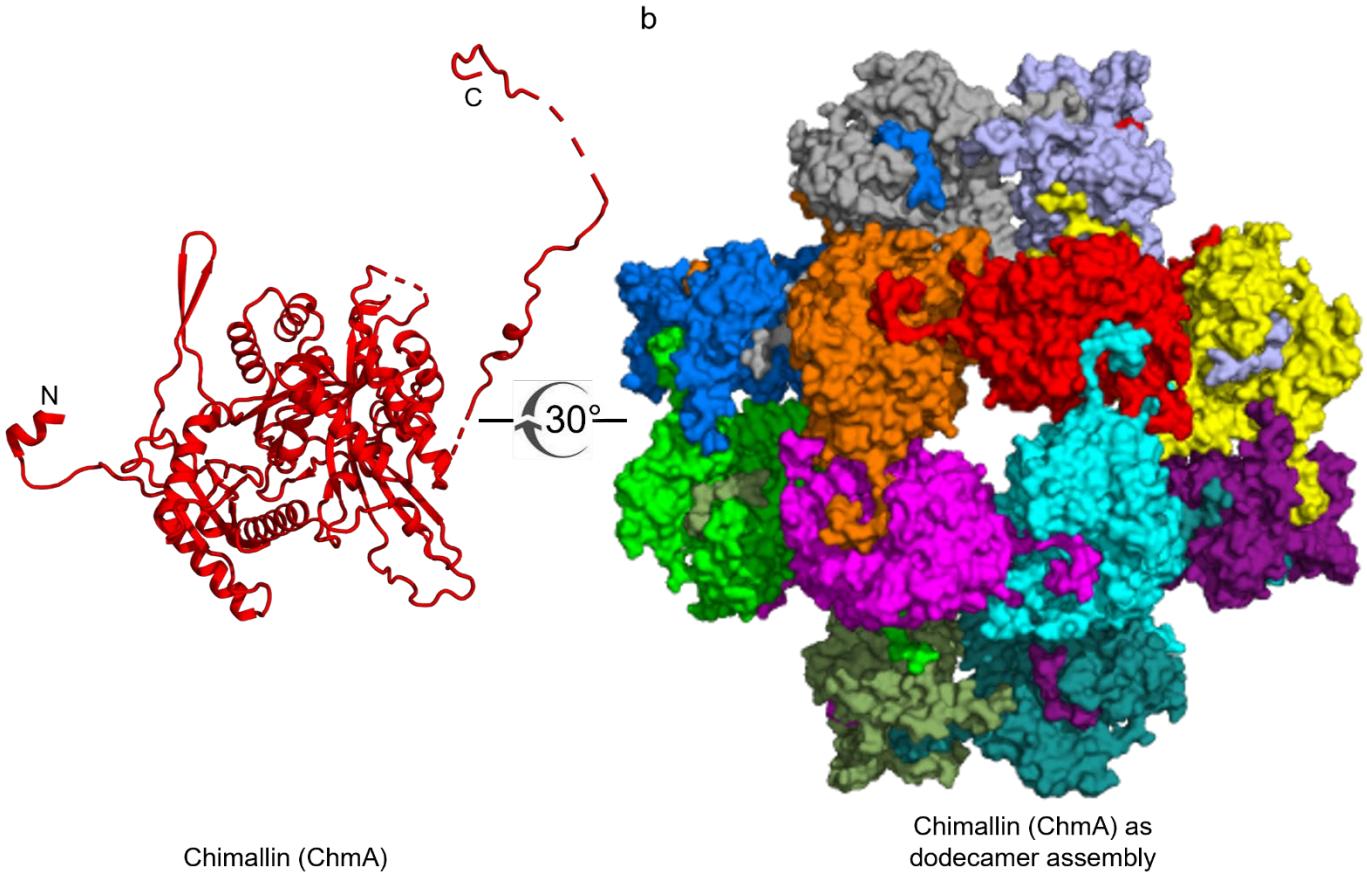

Figure S12. Changes in disorder in the self-assembling chimallin complex. The chimallin protomer self-assembles into an extremely large structure that encapsulates the bacteriophage genome. The structure of chimallin has only been determined in the context of the nuclear shell. **(a)** A resected protomer of chimallin highlights the lack of structure at both the N- and C-termini (PDB ID 7SQS)[16]. **(b)** The termini of each chimallin protomer interact with adjacent molecules in the nuclear shell (PDB ID 7SQQ)[16]. The high level of disorder and lack of secondary structure may provide plasticity, which can allow the nuclear shell to assemble[16-18].

Supplementary Figure 13

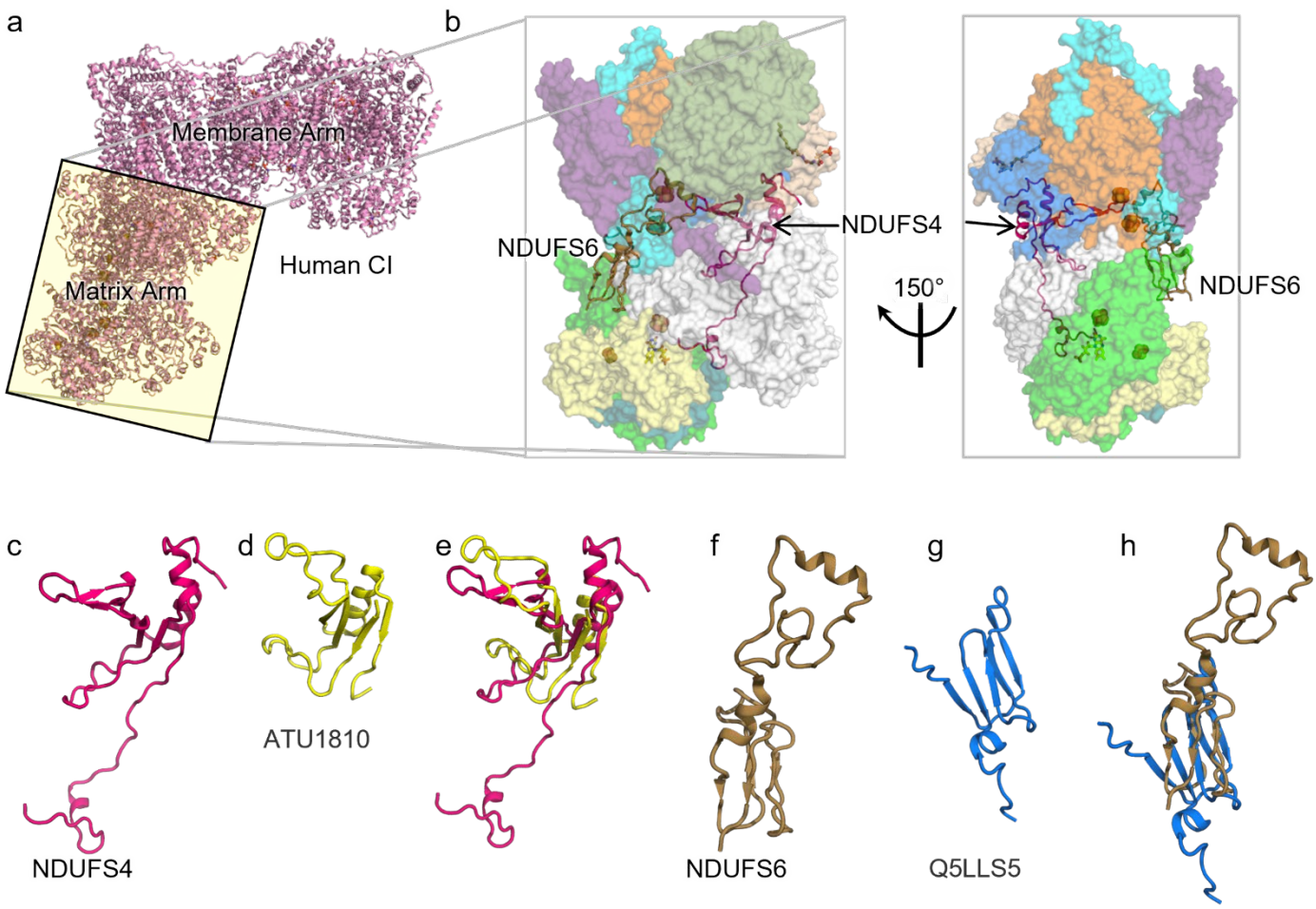

Figure S13. Disorder and flexibility in the accessory subunits of mitochondrial complex I.

(a) The cryoEM structure of human respiratory complex I (pink ribbon, PDB ID 5XTD)[19]. **(b)** Accessory subunits found in the matrix arm, which is the soluble region (PDB ID 5XTB)[19]. Two of these accessory subunits provide examples of disorder and dynamics in the assembly of complex. These are NADH dehydrogenase [ubiquinone] iron-sulfur protein 4 (NDUFS4, magenta ribbon) and NADH dehydrogenase [ubiquinone] iron-sulfur protein 6 (NDUFS6, brown ribbon). **(c)** In the context of assembled complex I, NDUFS4 (*hot pink*) is ordered but lacks secondary structure in >60% of the protein. **(d)** An NMR structure of a homolog from *Agrobacterium tumefaciens* (yellow ribbon, PDB ID 2JYA)[20], which shares 55% sequence similarity and 37% identity with residues 20-111 of NDUFS4. **(e)** NDUSF4 and the *A. tumefaciens* homolog fail to satisfyingly superpose. The RMS deviation of Cα atoms is > 5Å. The unstructured C-terminus of NDUSF4 is not observed in the structure of the bacterial homolog. **(f)** The structure of NDUFS6 resected from mammalian CI is ordered but lacks secondary structure in >70% of the protein. **(g)** The NDUFS6 homolog from *Silicibacter pomeroyi* (PDB ID 2JRR)[21] shares 67% sequence similarity and 43% identity with residues 80-119 of NDUFS6. **(h)** The NMR structure of the *S. pomeroyi* protein fails to superpose well with NDUFS6, with an RMS deviation of Cα atom of 4.8 Å.

REFERENCES

1 Sharma, P., Maklashina, E., Cecchini, G. & Iverson, T. M. The roles of SDHAF2 and dicarboxylate in covalent flavinylation of SDHA, the human complex II flavoprotein. *Proc Natl Acad Sci U S A* **117**, 23548-23556, doi:10.1073/pnas.2007391117 (2020).

2 Maklashina, E., Iverson, T. M. & Cecchini, G. How An Assembly Factor Enhances Covalent FAD Attachment to the Flavoprotein Subunit of Complex II. *J BIol Chem* **in press** (2022).

3 Rasband, W. S. (ed U.S. National Institutes of Health) (1997).

4 Eletsky, A. *et al.* Solution NMR structure of yeast succinate dehydrogenase flavinylation factor Sdh5 reveals a putative Sdh1 binding site. *Biochemistry* **51**, 8475-8477, doi:10.1021/bi301171u (2012).

5 Emsley, P. & Cowtan, K. Coot: model-building tools for molecular graphics. *Acta Crystallogr D Biol Crystallogr* **60**, 2126-2132, doi:10.1107/S0907444904019158 (2004).

6 Kudryavtseva, A. V. *et al.* Mutation profiling in eight cases of vagal paragangliomas. *BMC Med Genomics* **13**, 115, doi:10.1186/s12920-020-00763-4 (2020).

7 Sun, F. *et al.* Crystal structure of mitochondrial respiratory membrane protein complex II. *Cell* **121**, 1043-1057, doi:10.1016/j.cell.2005.05.025 (2005).

8 Furst, J. *et al.* ICln159 folds into a pleckstrin homology domain-like structure. Interaction with kinases and the splicing factor LSm4. *J Biol Chem* **280**, 31276-31282, doi:10.1074/jbc.M500541200 (2005).

9 Grimm, C. *et al.* Structural basis of assembly chaperone- mediated snRNP formation. *Mol Cell* **49**, 692-703, doi:10.1016/j.molcel.2012.12.009 (2013).

10 Abajian, C., Yatsunyk, L. A., Ramirez, B. E. & Rosenzweig, A. C. Yeast cox17 solution structure and Copper(I) binding. *J Biol Chem* **279**, 53584-53592, doi:10.1074/jbc.M408099200 (2004).

11 Banci, L. *et al.* A hint for the function of human Sco1 from different structures. *Proc Natl Acad Sci U S A* **103**, 8595-8600, doi:10.1073/pnas.0601375103 (2006).

12 Zhan, X., Gimenez, L. E., Gurevich, V. V. & Spiller, B. W. Crystal structure of arrestin-3 reveals the basis of the difference in receptor binding between two non-visual subtypes. *J Mol Biol* **406**, 467-478, doi:10.1016/j.jmb.2010.12.034 (2011).

13 Chen, Q. *et al.* Structural basis of arrestin-3 activation and signaling. *Nat Commun* **8**, 1427, doi:10.1038/s41467-017-01218-8 (2017).

14 Huang, W. *et al.* Structure of the neurotensin receptor 1 in complex with beta-arrestin 1. *Nature* **579**, 303-308, doi:10.1038/s41586-020-1953-1 (2020).

15 Staus, D. P. *et al.* Structure of the M2 muscarinic receptor-beta-arrestin complex in a lipid nanodisc. *Nature* **579**, 297-302, doi:10.1038/s41586-020-1954-0 (2020).

16 Laughlin, T. G. *et al.* Architecture and self-assembly of the jumbo bacteriophage nuclear shell. *Nature* **608**, 429-435, doi:10.1038/s41586-022-05013-4 (2022).

17 Chaikeeratisak, V. *et al.* Assembly of a nucleus-like structure during viral replication in bacteria. *Science* **355**, 194-197, doi:10.1126/science.aal2130 (2017).

18 Mendoza, S. D. *et al.* A bacteriophage nucleus-like compartment shields DNA from CRISPR nucleases. *Nature* **577**, 244-248, doi:10.1038/s41586-019-1786-y (2020).

19 Guo, R., Zong, S., Wu, M., Gu, J. & Yang, M. Architecture of Human Mitochondrial Respiratory Megacomplex I2III2IV2. *Cell* **170**, 1247-1257 e1212, doi:10.1016/j.cell.2017.07.050 (2017).

20 Lemak, A. *et al.* NMR solution structure of protein ATU1810 from Agrobacterium tumefaciens. Northeast Structural Genomics Consortium target AtR23, Ontario Centre for Structural Proteomics Target ATC1776. *Northeast Structural Genomics Consortium (NESG), Ontario Centre for Structural Proteomics (OCSP)*, doi:10.2210/pdb2JYA/pdb (2007).

21 Swapna, G. V. T. *et al.* Solution NMR Structure of Q5LLS5 from Silicibacter pomeroyi. Northeast Structural Genomics Consortium target SiR90. *Northeast Structural Genomics Consortium (NESG)*, doi:10.2210/pdb2JRR/pdb (207).